Sensors and Materials, Vol. 34, No. 7 (2022) 2663–2674
MYU Tokyo

S & M 2997

Geospatial Information Construction and Usability Evaluation Using Nadir Image and Oblique Image

Joon Kyu Park[1] and Keun Wang Lee[2*]

[1]Dept. of Civil Engineering, Seoil University, 28, Yongmasan-ro 90-gil, Jungnang-gu, Seoul 02192, Korea
[2]Dept. of Multimedia Science, Chungwoon University, 113, Sukgol-ro, Nam-gu, Incheon 22100, Korea

(Received November 6, 2021; accepted April 6, 2022)

Keywords: 3D modeling, accuracy analysis, geospatial information, nadir image, oblique image, ortho image

Recently, spatial information construction using drones has been employed in various fields such as aerial photogrammetry and ortho image production. Various types of drones for spatial information construction, such as fixed wing, rotary wing, and vertical takeoff and landing (VTOL) types, are being produced, and the field of application of drone photogrammetry is expanding as a result of intensive research. However, research on the construction and analysis of spatial information using oblique images is insufficient. In this study, geospatial information was constructed using a nadir image and an oblique image, and the utility of the oblique image was demonstrated through analysis. Accuracy was evaluated by comparing the accuracy of the ortho images obtained using the nadir image and oblique image with the Virtual Reference Station (VRS) survey result. As a result, accuracies of −0.024–0.017 and −0.023–0.031 cm were shown for the nadir image and oblique image, respectively, and the same accuracy as for the ground sample distance was confirmed. These results indicate that geospatial information constructed using oblique images can be employed for surveying, similarly to the results obtained using existing nadir images. Through additional research, it was possible to effectively perform 3D modeling of buildings using oblique images. The construction of geospatial information using an oblique image will be an effective way to create more realistic data.

1. Introduction

Recently, the field of application of geospatial information has been diversifying. In the past, medium-scale paper topographic maps were used for national land development, but with the development of technology, location-based services are expanding to digital large-scale navigation based on digital topographic maps, portal maps, ortho maps, and 3D maps. The development of digital technology has promoted the digital spatial information paradigm by digitizing various information generated in space, by building databases of the information, and by effectively classifying and utilizing information through software.[1,2] Geospatial information is opening up a new future with the 21st century IT technology. In the 2000s, the development of

*Corresponding author: e-mail: kwlee@chungwoon.ac.kr
https://doi.org/10.18494/SAM3728

ISSN 0914-4935

the IT industry environment was centered on wired and wireless communication technologies, and with the development of mobile services, spatial information rapidly emerged as a core service.[3,4] In the era of the Fourth Industrial Revolution, advanced intelligence such as drones, autonomous driving, artificial intelligence, big data, and IoT is increasing demand for up-to-date and high-quality national basic maps and ortho maps, which are the basis of national spatial information. In addition, drones are being used in various fields, such as construction, forest surveying, and search and rescue, as well as in the field of geospatial information, such as for topographic map and ortho image production. A drone is regarded as the most effective means of constructing geospatial information.[5] To increase the use of drones, the National Geographic Information Institute enacted the "Guidelines for Public Surveying Using Unmanned Aerial Vehicles" in March 2018 and is making continuous efforts to promote the use of unmanned aerial vehicles.[6]

Drones were developed mainly for military purposes, such as unmanned surveillance, reconnaissance, and mapping of enemy locations.[7] Although drones were first used in the field of spatial information about 30 years ago, they have only recently been widely used as a platform for data collection.[8] Photogrammetry by drones has enabled a variety of new applications to be pioneered in the field of close-up aerial photogrammetry.[9] As an alternative to existing photogrammetry by manned aircraft, such as low-cost, large-scale topographic map production and the acquisition of detailed 3D topographic information, it is becoming a complementary solution that can effectively acquire ground data. In addition to the proliferation of low-cost vehicles, the combination of non-measurement or digital cameras and the Global Navigation Satellite System (GNSS)/INS, which is capable of data acquisition, location prediction, automatic flight, and direct geo-referencing, has contributed to the successful development of drones in recent years.[10] Various studies such as on ortho image production and accuracy evaluation through drone photogrammetry have recently been conducted.[11] However, there have been relatively few photogrammetry studies using drone oblique images.

In this study, a nadir image and oblique image were acquired using drones, and a digital surface model (DSM) and ortho image were generated through data processing. An ortho image of the same target area was produced by each method, and the accuracy was evaluated. By comparing the results, the characteristics of the nadir image and oblique image were analyzed, and 3D modeling using the oblique image was performed to demonstrate its utility for constructing geospatial information. Figure 1 shows a flow of the study.

2. Drone Image Processing by SIFT Method

Although the image processing method has the advantage of being robust against changes in the contrast or exposure point, to detect extreme values in the scale space, it is necessary to apply the Laplacian filter to the Gaussian-filtered image. The scale-invariant feature transform (SIFT) method, developed to improve the detection of extreme values, has the advantage of a very high processing speed by approximating the Laplacian for each scale using the difference of Gaussians (DoG) rather than by directly calculating the Laplacian.[12] SIFT employs an image processing algorithm developed by Professor Matt Lowe of the University of British Columbia,

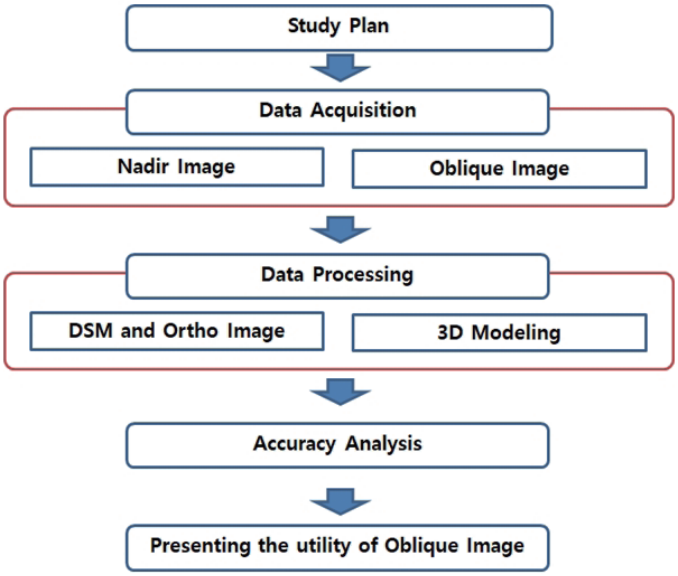

Fig. 1. (Color online) Study flow.

USA, and is a method of converting image data into feature points with local scale invariance. Since each converted feature point is invariant not only to scale and rotation, but also to changes in contrast and camera exposure, SIFT is the most suitable method for UAV image registration and is widely applied in most automatic aerial triangulation.[13] Feature point extraction using SIFT is usually performed in two steps. Step 1 is a feature point extraction step, which finds candidate feature points at various scales, then selects accurate feature points by examining the stability of the candidate feature points. Step 2 is the step of generating a descriptor for extracting the shape and characteristic information of the object. The direction component is obtained by calculating the gradient of the surrounding area based on the selected feature points, and interest is focused on the obtained direction component. A descriptor is created by resetting the area. To extract the scale-invariant feature points of the image, the scale space must first be created and the poles must be found there. The scale space refers to a space in which multiple images are created along the scale axis, in which the focus of the original image is blurred step by step by a blurring method. Blurring only changes the scale without directly enlarging or reducing the image. Since the original image has the same size (resolution), it is effective for understanding the image structure at a large scale. A representative scale space is an image pyramid, which is a series of image sets that are overlapped by reducing the size of the same image in stages.[14]

To create a scale space by blurring so that the image structure of the original image can be maintained without changing the position, a Gaussian filter must be applied. The Gaussian filter has the advantage that its shape remains unchanged in the space domain or frequency domain. The Gaussian filter is defined as the function

$$G(x,y,\sigma)=\frac{1}{2\pi\sigma^2}e^{-\left(x^2+y^2\right)/2\sigma^2}, \tag{1}$$

where σ is the scale vector. For the convolution operation, image L is an image blurred by applying a Gaussian filter to the original image $I(x, y)$, $L(x, y, \sigma) = G(x, y, \sigma) * I(x, y)$, and D, which is a DoG image, is defined as the difference between images to which a constant multiple of the Gaussian filter is applied as follows.

$$\begin{aligned} D(x,y,\sigma) &= \left[G(x,y,k\sigma) - G(x,y,\sigma) \right] * I(x,y) \\ &= L(x,y,k\sigma) - L(x,y,\sigma) \end{aligned} \tag{2}$$

Here, * is a convolution in the x and y directions, and the constant k is increased to gradually increase the degree of blurring of the original image using an ordinary multiplier.

In this way, if an image pyramid is created by superimposing multiscale spatial images using a Gaussian function, it is possible to find scale-invariant feature points.

A scale-invariant feature point is a feature point that can be found even if the scales of the input images are different from each other. It has the maximum cornerity within each scale image as well as the maximum cornerity on the scale axis; thus, the same feature point can be found at multiple scales. The basic principle of extracting feature points in SIFT is to calculate Laplacian values for each image scale, and select points as the feature points whose values are maximum (or minimum) not only within the image but also on the scale axis. Essentially, the Laplacian is an operator that calculates the curvature of an image brightness change. It has a minimum (or maximum) value at the point where the image brightness is locally maximum (or minimum). The Laplacian is the second derivative of the image brightness change and is calculated as

$$\begin{aligned} L = \nabla^2 I &= \frac{\partial^2 I}{\partial x^2} + \frac{\partial^2 I}{\partial y^2} \\ &= I(x+1y) + I(x-1y) + I(xy+1) + I(xy-1) - 4I(xy). \end{aligned} \tag{3}$$

A characteristic of the Laplacian is that it is close to zero where the brightness change of the image is constant, and it has a high value where the brightness change is abrupt, such as at the boundary of an area. However, if the Laplacian is calculated directly, the processing speed is reduced. Therefore, in SIFT, the Laplacian is approximated for each scale by using the DoG instead of directly calculating the Laplacian. The DoG refers to a subtraction image between adjacent images blurred by gradually applying a Gaussian filter to an input image, and theoretically obtains the same result as a Laplacian of Gaussian filter. The maximum or minimum in the DoG pyramid becomes the SIFT feature point. SIFT provides many feature points for image registration when there are fluctuations in image scale, rotation, contrast, camera exposure, and so forth. This becomes the basic data for the automatic aerial triangulation (AAT) process for drone image processing. Therefore, it is possible to perform the AAT step after automatically splicing drone images using the SIFT method.

3. Data Acquisition

In this study, the whole of Gyeonggi-do was selected as a research target to construct spatial information using a nadir image and oblique image obtained with drones. The study site was selected as an area of about 700 m × 700 m including flat land, buildings, and forests. Figure 2 shows the study area and Fig. 3 shows an overview of the study area.

Data for photogrammetry were acquired using Wingtra's vertical takeoff and landing (VTOL) drone. The shooting plan for photogrammetry was set to automatic flight, taking into account the longitudinal and lateral overlaps at an altitude of 150 m, and data were acquired for each sensor. Figure 4 shows the VTOL drone and Table 1 shows its specifications.[15]

RX1A2 and A6100 cameras were used for image acquisition. The sensor information for each camera is shown in Table 2.

The flight mission was performed using Wingtra Pilot software. The flight altitude was 150 m, and the longitudinal and lateral overlaps were set at 80%. The shooting time was 30 min, and 377 photographs were taken to capture the nadir image and 244 photographs were taken to capture the oblique image. The difference in the number of photographs between the nadir and oblique images is because the angle of view is different. Since the oblique image has a relatively large angle of view, fewer pictures were acquired. Figure 5 shows the mission planner screen for the flight mission and Fig. 6 shows part of the actual flight trajectory.

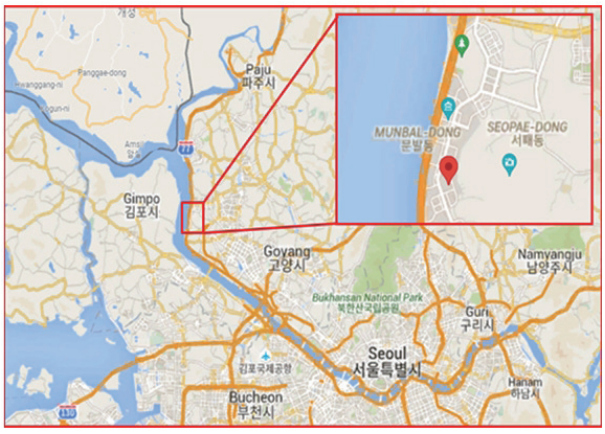

Fig. 2. (Color online) Study area.

Fig. 3. (Color online) Overview of the study area.

Fig. 4. (Color online) VTOL drone.

Table 1
Specifications of the drone.

Type	VTOL
Weight	4.5 kg
Resolution of CCD	42 MP (nadir 90º) / 24 MP (oblique 66º)
Wingspan	125 cm
GNSS	Two-frequency GNSS
Flight Speed	64.8 km/h
Flight Time	1 h
Mission Planner	Android

Table 2
Image sensor information.

Item	RX1A2	A6100
ISO	100-25600	100-32000
Lens	ZEISS 35 mm f2.0 Sonnar T	Sony E-mount Lenses 15 mm
Sensor	Exmor CMOS	APS-C Exmor CMOS

Fig. 5. (Color online) Mission planner screen.

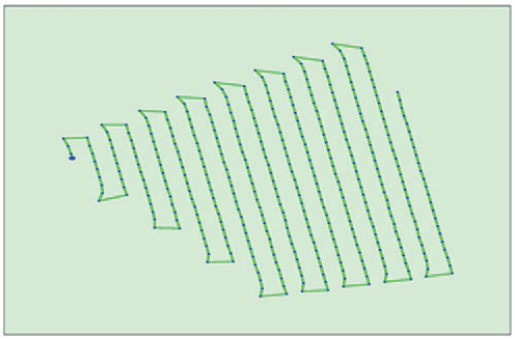

Fig. 6. (Color online) Part of the actual flight trajectory.

4. Data Processing and Analysis

The data collected by the drone consist of the photographs taken and the exterior orientation (EO) of each photograph. In this study, photographs and EO values were used for data processing. Because Wingtra stores geotagged photographs, these values were used for data processing. The software used for ortho image and DSM production was Pix4D Mapper. The data processing was performed in the order of data import, tie point extraction, ground control point (GCP) measurement, orientation, and result generation. Figures 7 and 8 respectively show the data processing process and software screen. Five GCPs were used for data processing, whose coordinates are shown in Table 3.

Table 4 shows the absolute camera position and orientation uncertainties calculated from the orientation results. From the sensor orientation results, it was found that the nadir sensor showed more precise values than the oblique sensor (Fig. 9).

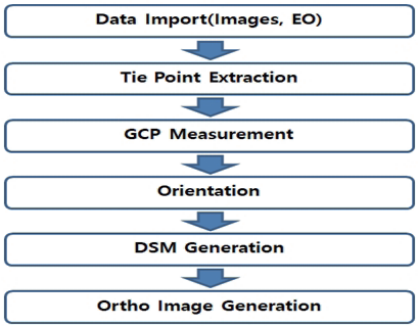

Fig. 7. (Color online) Data processing flow.

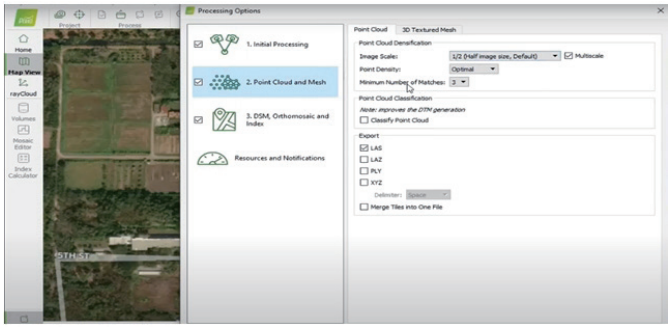

Fig. 8. (Color online) Data processing screen.

Table 3
Coordinates of GCPs.

No.	N (m)	E (m)	H (m)
1	566799.065	172366.580	4.627
2	567176.159	172796.601	16.507
3	566635.908	172858.384	11.957
4	566807.391	172664.102	5.710
5	566527.331	172666.093	5.017

Table 4
Absolute camera position and orientation uncertainties.

Item	Nadir		Oblique	
	Mean	Sigma	Mean	Sigma
X (m)	0.204	0.048	0.020	0.004
Y (m)	0.229	0.093	0.028	0.007
H (m)	0.291	0.048	0.022	0.004
Omega (degree)	0.080	0.044	0.010	0.002
Phi (degree)	0.063	0.028	0.007	0.002
Kappa (degree)	0.033	0.031	0.002	0.002

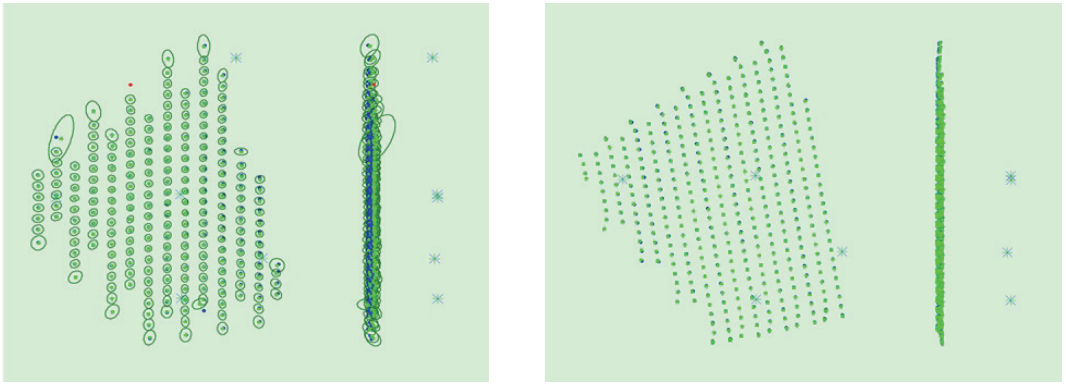

(a) (b)

Fig. 9. (Color online) Uncertainty ellipses (100× magnification). (a) Nadir image. (b) Oblique image.

Through data processing, DSM and ortho images were generated as nadir images and oblique images. Figures 10 and 11 show the data processing results.

In the case of using a DSM and ortho image, a wider area was obtained when oblique images were used than when nadir images were used. This is because the angle of view of the oblique images was larger than that of the nadir images, so the shooting area was wider. The focal length of the nadir images was 35 mm, that of the oblique images was 24 mm, the ground sample distances (GSDs) of the images acquired at 150 m altitude were 2 and 3 cm, and the resolution of the nadir images was high. As shown in Fig. 10(b), in the case of DSM using oblique images, it can be seen that the side of the building was more completely constructed. This is considered to be because there are more images of the side of the building among the oblique images than among the nadir images. The oblique image faces the rear at an angle of 66°, and owing to the overlap of 80%, most of the side of the building appears in the photograph. Figure 12 shows a comparison between the nadir image and the oblique image.

The accuracies of the nadir image and oblique image were evaluated using a check point (CP). The coordinates of the CP were acquired by a GNSS survey using the virtual reference

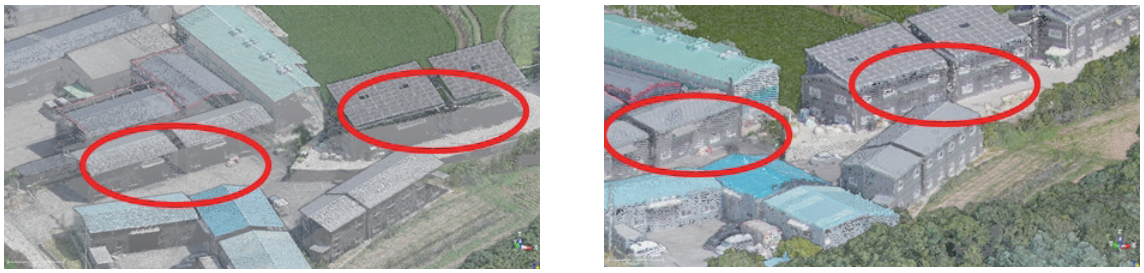

(a) (b)

Fig. 10. (Color online) DSM. (a) Nadir image. (b) Oblique image.

(a) (b)

Fig. 11. (Color online) Ortho image. (a) Nadir image. (b) Oblique image.

(a) (b)

Fig. 12. (Color online) Comparison between (a) nadir image and (b) oblique image.

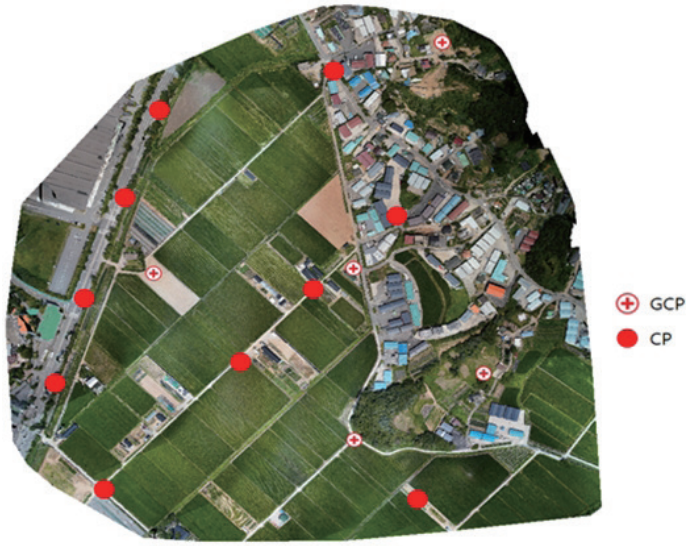

Fig. 13. (Color online) Locations of GCPs and CP.

station (VRS) method. Road lanes and features were used, and the accuracy was evaluated by comparing the VRS performance with the performance obtained from each ortho image. Figure 13 shows the locations of the GCPs and CP. Table 5 shows results of the accuracy analysis.

According to the accuracy analysis, the nadir image showed an accuracy of −0.024–0.017 cm and the oblique image showed an accuracy of −0.023–0.031 cm. These results can be viewed within each GSD, indicating that accuracy of about one pixel can be secured even when an oblique image is used. Figure 14 shows a comparison of the deviations of the nadir image and the oblique image. Unfortunately, an ortho image obtained using an oblique image in some building areas showed the side of the building, so it was not possible to obtain an accurate ortho image. However, there was no significant difference from the ortho image obtained using the nadir image in areas other than the building. Figure 15 shows the difference between the nadir image and the oblique image appearing in the building.

Table 5
Results of accuracy analysis.

No.	VRS		Nadir image		Oblique image	
	N (m)	E (m)	dN (m)	dE (m)	dN (m)	dE (m)
1	567078.012	172376.724	−0.012	0.014	0.024	−0.021
2	566933.452	172326.241	0.011	0.021	0.026	−0.021
3	566764.214	172262.875	0.014	0.011	0.027	−0.022
4	566632.322	172219.224	−0.018	0.012	0.029	−0.022
5	566452.899	172290.650	−0.024	0.018	−0.014	−0.023
6	566664.610	172498.980	−0.021	0.016	0.021	−0.014
7	566777.750	172609.115	−0.019	0.015	0.023	0.026
8	566901.110	172733.332	−0.019	0.015	0.021	0.028
9	567127.884	172633.324	−0.021	0.017	0.021	0.026
10	566435.551	172762.214	0.017	0.021	0.023	0.031
	RMSE		0.016	0.003	0.012	0.025

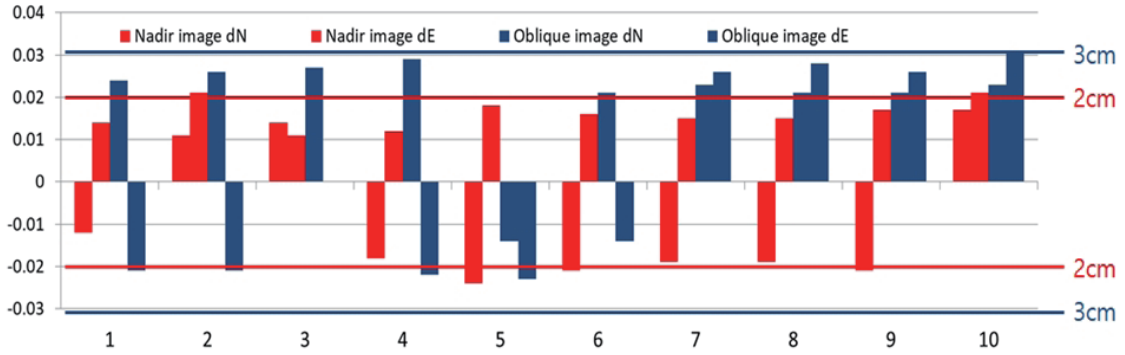

Fig. 14. (Color online) Comparison of deviations of nadir image and oblique image.

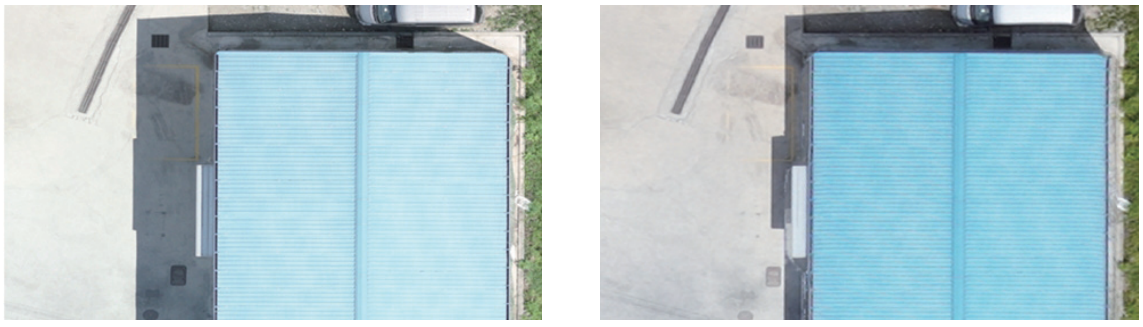

(a) (b)

Fig. 15. (Color online) Difference between (a) nadir image and (b) oblique image appearing in the building.

In this study, 3D modeling of buildings and terrain was performed using DSM with oblique images, and texture mapping was performed using photographs of the side and top of the building. Figure 16 shows the results of 3D modeling using the oblique images.

Fig. 16. (Color online) Results of 3D modeling using oblique image.

It was found that using an oblique image enables more realistic modeling of a building or topography than using a nadir image. The results of this study suggest that it is possible to produce an orthogonal image with the same accuracy as GSD by using an oblique image, indicating that an oblique image is more suitable for 3D modeling than a nadir image. The use of an oblique image can simplify the existing 3D modeling of features such as buildings and reduce the number of separate photographs taken for texture mapping, and if an oblique image is used for visualization of the real world using geospatial information, the work efficiency can be improved.

5. Conclusion

In this study, geospatial information was constructed using a nadir image and an oblique image, and the utility of the oblique image was demonstrated through analysis. Images of the study site were acquired by each method at an altitude of 150 m, and DSM and ortho images were generated through data processing. In the case of DSM and ortho images, a wider area was obtained when oblique images were used than when nadir images were used. It was also possible to create a more detailed DSM for the side of a building. Accuracy was evaluated by comparing the accuracy of the ortho images obtained using the nadir image and oblique image with the VRS survey result. As a result, accuracies of −0.024–0.017 and −0.023–0.031 cm were shown for the nadir image and oblique image, respectively, and the same accuracy as the GSD was confirmed. These results indicate that geospatial information constructed using oblique images can be employed for surveying, similarly to the results obtained using existing nadir images. Through additional research, it was possible to effectively perform 3D modeling and texture mapping of buildings using oblique images. As a result, it was possible to create data that can represent the real world more visually.

Acknowledgments

This research was supported by the Basic Science Research Program through the National Research Foundation of Korea (NRF) funded by the Ministry of Science and ICT (No. NRF-2021R1F1A1061677).

References

1 J. Y. Cho, J. I. Song, C. R. Jang, and M. Y. Jang: J. Korea Acad.-Ind. Coop. Soc. **21** (2021) 372. https://doi.org/10.5762/KAIS.2020.21.10.372
2 J. W. Lee, D. P. Kim, and S. M. Sung: J. Korea Acad.-Ind. Coop. Soc. **21** (2021) 197. https://doi.org/10.5762/KAIS.2020.21.10.197
3 I. S. Lee: J. Korea Acad.-Ind. Coop. Soc. **22** (2021) 268. https://doi.org/10.5762/KAIS.2021.22.3.268
4 Q. Qi, F. Tao, T. Hu, N. Anwer, A. Liu, Y. Wei, L. Wang, and A. Y. Nee: J. Manuf. Syst. **58** (2021) 372. https://doi.org/10.1016/j.jmsy.2019.10.001
5 H. S. Jamg, J. H. Go, and H. S. Jang: J. Korean Soc. Geospatial Inf. Sci. **25** (2017) 47. https://doi.org/10.7319/kogsis.2017.25.4.047
6 National Geographic Information Institute: http://ngii.go.kr/ (accessed September 2021).
7 J. Y. Chung: J. Korea Acad.-Ind. Coop. Soc. **21** (2021) 119. https://doi.org/10.5762/KAIS.2020.21.1.14
8 Y. H. Shin, K. W. Sohn, S. B. Lim, and D. C. Lee: J. Korean Soc. Surv. Geodesy Photogramm. Cartogr. **39** (2021) 223. https://doi.org/10.7848/ksgpc.2021.39.4.223
9 K. J. Ahn and D. S. Ko: J. Digital Contents Soc. Content **20** (2019) 208. https://doi.org/10.9728/dcs.2019.20.1.119
10 J. K. Park and K. Y. Jung: J. Korean Soc. Surv. Geodesy Photogramm. Cartogr. **39** (2021) 47. https://doi.org/10.7848/ksgpc.2021.39.1.47
11 K. R. Lee, Y. K. Han, and W. H. Lee: Korea Soc. Geospatial Inf. Sci. **26** (2018) 23. https://doi.org/10.7319/kogsis.2018.26.3.023
12 S. I. Baek, S. Y. Koh, and W. K. Kim: J. Korean Soc. Surv. Geodesy Photogramm. Cartogr. **38** (2020) 707. https://doi.org/10.7848/ksgpc.2020.38.6.707
13 I. Stamos, L. Liu, C. Chen, G. Woldberg, G. Yu, and S. Zokai: Int. J. Comput. Vision **78** (2008) 237. http://dx.doi.org/10.1007/s11263-007-0089-1
14 D. Lowe: Proc. Int. Conf. Computer Vision (1999) 1–8. https://doi.org/10.1109/ICCV.1999.790410
15 Wingtra, WingtraOne: https://www.Wingtra.com/ (accessed September 2021).